The WRF nested within the CESM: Simulations of a midlatitude cyclone over the Southern Great Plains

Juanxiong He,[1] Minghua Zhang,[1] Wuyin Lin,[2] Brian Colle,[1] Ping Liu,[1] and Andrew M. Vogelmann[2]

[1] This paper describes an integrated modeling system in which the Weather Research and Forecasting model (WRF) is nested within the Community Earth System Model (CESM). This system is validated for the simulation of a midlatitude cyclongesis event over the Southern Great Plains of the United States. The global atmospheric model CAM4 at T42 resolution in the CESM has missed this cyclogenesis, while the nested WRF at 30 km grid spacing (or finer) that is initialized with the CAM4 condition and laterally forced by the CAM4 successfully simulated the deepening midtropospheric trough and associated cyclogenesis. An analysis of the potential velocity evolution and sensitivity experiments show that it is the higher WRF resolution that allowed the realistic sharpening of the Ertel's Potential Vorticity (EPV) gradient and the ensuing cyclogenesis. The terrain resolution and the physical parameterizations, however, play little role in the difference between the CAM4 and the WRF in the CESM. The integrated WRF/CESM system is intended as one method of global climate modeling with regional simulation capabilities. The present case study also serves as a verification of the system by comparing with standalone WRF simulations forced by operational analyses.

Citation: He, J., M. Zhang, W. Lin, B. Colle, P. Liu, and A. M. Vogelmann (2013), The WRF nested within the CESM: Simulations of a midlatitude cyclone over the Southern Great Plains, *J. Adv. Model. Earth Syst.*, 5, doi:10.1002/JAME.20042.

1. Introduction

[2] Future climate changes are generally simulated and projected by global climate models [*Randall et al.*, 2007; *Taylor et al.*, 2012]. Understanding how these changes will manifest themselves at regional scales is in high demand by the society, because it is the changes of the weather events at regional scales that are most relevant to impact studies and to mitigation and adaption strategies. However, due to the prohibitive computational costs, the current operational global climate models, such as those in the Coupled Model Intercomparison Project Phase 5 (CMIP5) [*Taylor et al.*, 2012], still cannot resolve the high-impact weather events (e.g., heavy precipitation, strong winds, and urban heat waves) that are essential to regional climate.

[3] To bridge the gap between global models and societal demands, regional climate models (RCMs) have been developed to downscale global model results at high resolution in limited areas [e.g., *Dickinson et al.*, 1989]. Since surface topography can play an important role in regional climate, the high-resolution RCMs may produce better simulations of climate in regions with complex terrain [*Anthes et al.*, 1989; *Giorgi*, 1990]. The RCMs, however, require lateral boundary forcing from the global models; thus uncertainties of the global model can impact the regional simulations, and this has been the subject of scrutiny since the birth of the regional climate modeling [*Giorgi*, 1990, 1995; *Cocke and LaRow*, 2000]. Ideally, the RCMs should also serve to improve the global model in addition to provide regional climate information.

[4] There are several plausible approaches to obtain regional climate information with high resolution. One is high-resolution modeling over the whole globe [e.g., *DeWeaver and Bitz*, 2006; *McClean et al.*, 2011]. The second is the global model with a regional mesh refinement [*Taylor and Fournier*, 2010]. The third is RCM nested within global model with two-way interaction or one-way simulations [e.g., *Leung et al.*, 2006]

[5] We pursue the approach in which the mesoscale Weather Research and Forecasting (WRF) model is nested within the global Community Earth System Model (CESM). Since both models are widely used in the community [*Gent et al.*, 2011; *Michalakes et al.*, 2004; *Craig et al.*, 2011], this combination enables us to potentially make use of the large body of literature and development efforts for regional climate studies. Many previous studies have employed the WRF to downscale results from global models such as the Community Atmosphere Model (CAM) [e.g., *Bukovsky and Karoly*,

[1]School of Marine and Atmospheric Sciences, State University of New York at Stony Brook, Stony Brook, New York, USA.
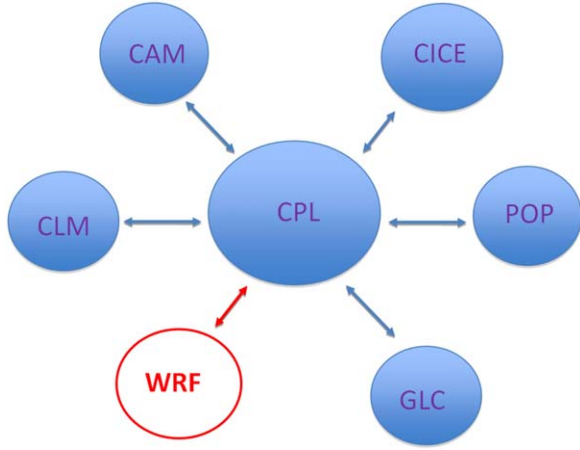[2]Brookhaven National Laboratory, Upton, New York, USA.

Figure 1. Schematic of WRF nested within the CESM, where WRF communicates with other component models of the CESM through the coupler (CPL). The CESM component models shown are the Community Atmosphere Model (CAM), Community Land Model (CLM), Parallel Ocean Program (POP), sea-ice model (CICE), and the land-ice model (GLC).

2011; *Jin et al.*, 2011; *Xu and Yang*, 2012], our effort differs by integrating WRF into CAM as a single modeling system, so that WRF results can be considered as regional simulations from the global model. While our ultimate goal is to develop a model with two-way coupling, in this paper, we describe a system with WRF nested inside the CESM through one-way coupling and use it to investigate a cyclogenesis event over the Southern Great Plains (SGP) of the United States during the March 2000 Intensive Observation Period (IOP) of the Atmospheric Radiation Measurement (ARM) Program. Methodologically, this integrated system in one-way coupling is the same as standard downscaling method, except that the nested model shares the same initial condition as the host model. However, the integrated system allowed us to easily evaluate the difference between the WRF and CAM4 and to conduct sensitivity studies with respect to their respective surface conditions such as topography, as what will be reported in later sections. The one-way study is intended as a stepping stone to two-way nesting that will include upscale feedbacks so that regional simulation can improve global model results.

[6] The objective of this paper is to assess the feasibility and capability of such a system in simulating cyclogenesis and to analyze the cause of the improvement of the nested WRF simulation relative to the global model alone, because middle-latitude cyclones are one of the dominant weather systems that can cause flooding, wind gusts, and other severe weather phenomena. The ability of a model to simulate cyclogenesis is a necessary condition for it to provide credible regional climate information for a global modeling system.

[7] In section 2, we introduce the integrated WRF/ CESM modeling system along with the experimental setup for the case study. In section 3, we briefly describe the cyclogenesis event. In section 4, we show results from the integrated modeling system and analyze cause of the difference in model results. The last section contains a summary.

2. Modeling System and Experimental Setup

2.1. The Integrated WRF/CESM System

[8] The WRF/CESM modeling system is developed from the CESM Version 1.0 and the Advanced Research WRF (ARW) Version 3.2. Different from the common practice of running the WRF by using offline lateral boundary conditions from operational analyses or global models, in the WRF/CESM system, the CAM within the CESM provides the lateral atmospheric boundary conditions online to the WRF, and CAM also provides the initial conditions, surface temperature, and soil moisture to drive WRF. The modeling system is designed for WRF to feedback to CAM through the CESM coupler, but the methodology of the upscaling feedback is still being investigated, so the present study only shows results of the WRF driven by the CAM and results from the CAM itself. Thus the WRF acts as a regional downscaling model inline of the CESM that shares the initial condition with the CAM. Note that the integrated system can use either CAM4 or CAM5 as the global atmospheric component. In this study, CAM4 in the CESM is adopted. Figure 1 shows a schematic of the modeling system, in which WRF is a component model of the CESM. It should be pointed out that, in this system, WRF does not replace CAM, as is done for the coupled WRF in the Regional Arctic Climate Model [*He et al.*, 2009; M. E. Higgins et al., The Regional Arctic Climate Model (RACM): Atmospheric implementation and validation, submitted to *Journal of Climate*, 2013). Instead, WRF provides additional information on top of CAM. The WRF/CESM system, however, can be configured as a regional climate model driven by reanalysis fields as the lateral boundary.

[9] The data exchange between the WRF and CAM are achieved through the CESM Coupler Version 7 (CPL7). An alternative coupling strategy is to carry out data exchange inside the CAM, treating WRF as part of CAM instead of CESM. We did not choose this method because through the Coupler, WRF fields can be also made available to the ocean, land, sea-ice models and vice versa for future development.

[10] To construct the WRF/CESM system, WRF and CESM are modified at the coding level. For the WRF, the most important modification is the integration of the WRF Preprocessing System (WPS) into the ARW as a single component. Other modifications to the WRF include the following: (i) restructuring of the top software layer to control model integrations; (ii) synchronization of the WRF time manager with the CESM time manager; (iii) relocation of parallel initialization; (iv) configuration of the WRF domain structure in CESM. For the CESM, new variables, data structures, and subroutines are introduced into the main driver and CPL7; these include data structures to store the
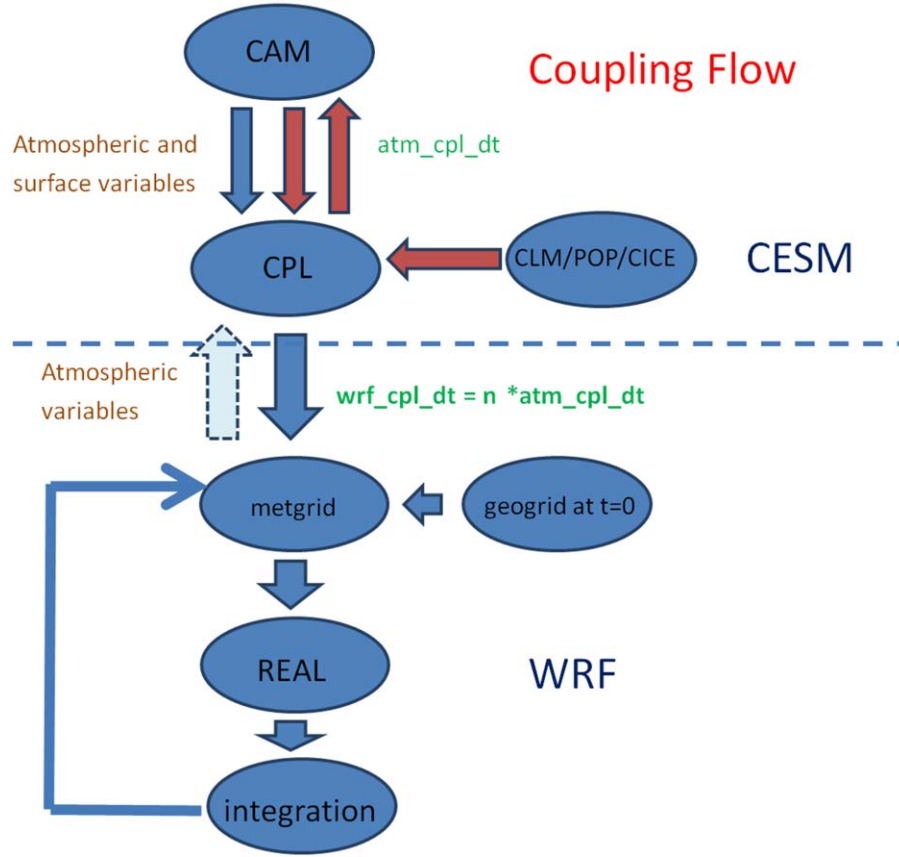
Figure 2. Schematic of the integration of WRF into the CESM. The METGRID and GEOGRID programs in the WRF Preprocessing System (WPS) and the REAL program are combined with WRF as a single submodel of the CESM. wrf_cpl_dt is the coupling time interval of the WRF with CPL7; atm_cpl_dt is the coupling interval of CAM with CPL7 within CESM. wrf_cpl_dt is designed as an integer multiple of atm_cpl_dt. In the study, wrf_cpl_dt is 6 h and atm_cpl_dt is 20 min.

three-dimensional data of WRF and CAM, and modules to receive and send data between WRF and CPL7 as well as between CAM and CPL7. To facilitate the synchronization, the time managers in both CESM and WRF are revised to use the Earth System Model Framework (ESMF) library.

[11] Figure 2 shows a schematic of the time integration of WRF in the CESM. For the WRF component at the initialization time of the CESM integration, the surface terrain height, land/sea mask, vegetation type, land use category, and albedo are obtained from the external geophysical data sets provided by the WRF development team. At the initial time step, WRF also receives the three-dimensional atmospheric state variables (winds, temperature, and humidity) and two-dimensional surface fields from the coupler to generate initial conditions and lateral boundary conditions by using the online preprocessing system. The WRF is therefore initialized based on, and forced by, the CAM atmospheric fields. The frequency of data exchange between the WRF and the coupler can be set either to every CAM time step, or to any specified length of time as long as it is an integer multiple of the WRF and CAM time steps. WRF is integrated within each data

exchange step, at the beginning of which WRF updates its lateral boundary data set, sea surface temperature, and sea ice from the CESM. During the integration of the system, CAM leads WRF by one coupling time interval. Table 1aa lists the fields that WRF receives from CPL7. Table 1bb lists the fields that WRF exports to CPL7, even though the latter are not yet used by the CAM.

2.2. Experimental Setup

[12] The integrated WRF/CESM system was used to simulate a cyclogenesis event described in the next section. We use a time interval of 6 h for data exchanges

Table 1a. Variables Imported by WRF From CPL7

Type	Variables
Surface	Snow depth, surface skin temperature, coarse CAM terrain, land mask, sea surface temperature, sea ice mask, surface pressure, sea level pressure
Soil	Soil temperature and soil moisture
Atmosphere	Zonal wind, meridional wind, temperature, relative humidity, geopotential height and pressure on each vertical level of CAM

Table 1b. Variables Exported by WRF to CPL7

Type	Variables
Atmospheric state variables	Three-dimensional zonal wind, meridional wind, temperature, and specific humidity
Atmospheric tendency variables	Three-dimensional temperature tendency due to physical processes and three-dimensional specific humidity tendency due to physical processes

between WRF and CPL so that the simulation results can be compared with the standalone ARW simulations driven by 6 hourly National Center for Environmental Prediction (NCEP) Global Forecasting System (GFS) analyses at the boundaries. The CESM used data ocean and the prescribed sea-ice models (DOCN7 and DICE4) but active land and atmospheric models CLM4 and CAM4, with the CAM using the T42 spectral dynamical core. We added an initialization module for the CAM4 and CLM4 to allow for case study simulation. The initial conditions for CAM4 were generated by interpolating the NCEP GFS $1° \times 1°$ data to the T42 Gaussian grids by using the first-order area-weighted mapping. CLM4 was spun up by using the atmosphere data model in CESM (DATM7) and the surface forcing of *Qian et al.* [2006] for 10 years up to the starting date and time of the experiment. Sea surface temperature and sea ice data are from the National Oceanic and Atmospheric Administration (NOAA) Optimum Interpolation sea surface temperature V2 (NOAA_OI_SST_V2) data set provided by the National Oceanic and Atmospheric Administration/Ocean and Atmospheric Research/Earth System Research Laboratory (NOAA/OAR/ESRL) available at http://www.esrl.noaa.gov/psd/ [*Reynolds et al.*, 2002], whose temporal resolution is weekly and spatial resolution is $1° \times 1°$.

[13] The WRF domain covers North America and part of the Pacific and Atlantic oceans. Table 2 lists the experiments and their specifications of grid and domain as well as the configurations of the WRF. E_CTL, and E_ARW, respectively, represent WRF nested within CESM and WRF driven by GFS analyses. They will be used to assess the integrated modeling system. E_Terrain is an experiment in which the high-resolution surface terrain in the nested WRF is replaced by the coarse-resolution terrain of CAM4 to study the impact

of terrain on the results. E_Physics is designed to study the impact of physical parameterizations. E_Res1 and E_Res2 are designed to study the impact of the WRF model resolution on the results.

[14] In all the experiments, WRF has 31 vertical levels with its top at 50 hPa. The third-order Runge-Kutta (RK3) time integration scheme is employed to integrate the equations. The WRF physics used the CAM long-wave and shortwave radiation scheme [*Collins et al.*, 2004], Kain-Fritsch cumulus scheme [*Kain*, 2004], WRF Single-Moment (WSM) 3-class microphysics scheme [*Hong et al.*, 2004], Yonsei University planetary boundary layer (YSU PBL) scheme [*Hong et al.*, 2006], Monin-Obukhov surface layer scheme [*Grell et al.*, 1994], and NOAH land surface scheme [*Chen and Dudhia*, 2001]. The CAM4 also has 31 vertical levels, but they are in a hybrid-pressure coordinate that is different from the WRF sigma coordinate. The CAM4 standard suite of physical parameterizations was used (R. B. Neale et al., The mean climate of the community atmosphere model (CAM4) in forced SST and fully coupled experiments, submitted to *Journal of Climate*, 2012). [U.S. National Centers for Environmental Prediction et al., 2000] The NCEP GFS $1° \times 1°$ analysis data sets and the daily Global Precipitation Climatology Project (GPCP) precipitation data sets are used to evaluate the results [University Corporation for Atmospheric Research (UCAR) online] [*Adler et al.*, 2003].

3. Case Description

[15] The cyclone event occurred during the ARM March 2000 Intensive Observational Period (IOP). This case was also studied by the ARM Cloud Modeling and Parameterization Working Group for cloud simulations by using Single-Column Models (SCMs) and Cloud Resolving Models (CRM) [*Xie et al.*, 2005; *Xu et al.*, 2005].

[16] From 1 March 2000 to 4 March 2000, a midlevel trough along the U.S. west coast developed into a cutoff low as it moved eastward, which was associated with surface cyclogenesis and heavy precipitation over the ARM Southern Great Plains (SGP) site. Figures 3a–3e show the evolution of the 500 hPa geopotential heights from the NCEP GFS analysis. Figure 3a is for 00 universal coordinated time (UTC) of 1 March that will be used as the initial condition of model simulation in the next section. Figures 3b–3d are the geopotential heights

Table 2. The Experiment Configurations

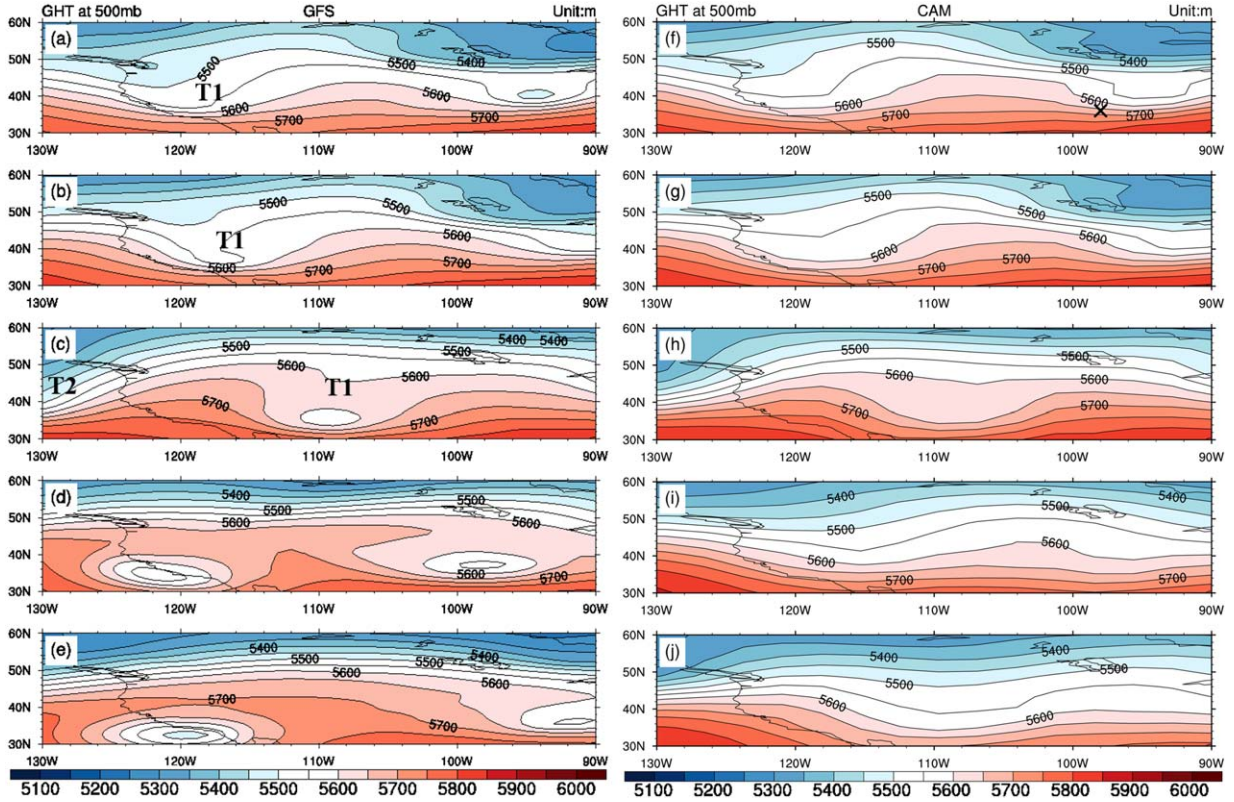|	Resolution	Domain	Terrain Source	Configuration
E_CTL	30 km $\times$ 30 km	400 $\times$ 280	USGS 30s data	CAM long-wave and short-wave
E_ARW	30 km $\times$ 30 km	400 $\times$ 280	USGS 30s data	scheme, Kain-Fritsch cumulus
E_Terrain	30 km $\times$ 30 km	400 $\times$ 280	CAM T42	scheme, YSU PBL scheme,
E_Res1	2.5° $\times$ 2.5°	123 $\times$ 25	USGS 30s data	WSM 3-class microphysics scheme, Monin-Obukuhov surface layer scheme, NOAH land surface scheme
E_Res2	10 km $\times$ 10 km	1202 $\times$ 842	USGS 30s data	No cumulus scheme
E_Dry	30 km $\times$ 30 km	400 $\times$ 280	USGS 30s data	No microphysical and cumulus scheme

Figure 3. Geopotential heights at 500 hPa, unit: meter. Each plot from top to bottom is for 00 UTC for 1 March, 06 UTC for 1–3 March, and 00 UTC for 4 March. (a–e) NCEP GFS and (i–j) CAM4. T1 in Figure 3a corresponds to the trough over the California coast. T2 corresponds to the trough just off the west coast. The black bold marker "cross" in Figure 3f is the center of the ARM SGP site.

at 06 UTC of each day except that Figure 3e is at 00 UTC of 4 March. The following features are noted and they will be used to discuss the model results. At 0000 UTC 1 March (Figure 3a), a trough is located at the California coast (referred to and labeled as T1 in later discussions). About 1500 km upstream of this trough is another broad trough over the North Pacific (referred to as T2). T1 deepens in the first 6 h. By 0600 UTC 2 March (Figure 3c), a cutoff low develops near (35°N, 110°W), which corresponds to the surface cyclogenesis to the east of the Rocky Mountain [*Wu et al.*, 2007]. By 0600 UTC 3 March (Figure 3d), the cutoff low center is over the ARM SGP. This low center moves away from the SGP on 4 March, which corresponds to the passage of a surface cold front and associated heavy precipitation over the SGP (not shown).

[17] Another trough in the North Pacific (T2) also moves eastward close to the west coast from 1 March to 2 March. Over the next few days, T2 intensified and became stationary at the California coast, creating a ridge over the SGP and fair weather after 4 March. Our primary focus will be on the evolution of T1.

4. Results

4.1. Simulation of Cyclogenesis

[18] Figures 3f–3j show the evolution of the 500 hPa geopotential height simulated by CAM4. The model

was well initialized by the GFS analysis at 0000 UTC 1 March (Figures 3a and 3f) but, during the following 3 days, the trough (T1) in CAM4 did not amplify into the cutoff low seen in the GFS. As a result, the model only simulated weak precipitation over SGP (Figures 4a and 4b) due to the passage of a trough that is much weaker than observed. Also, the simulated propagation speed of T1 over the SGP is faster than observed, as can be seen in Figures 3d–3e and 3i–3j. CAM4 also missed the development of T2 into a closed low by 0600 UTC 3 March.

[19] Meanwhile, the nested WRF forced by CAM4 by using the same initial conditions in the WRF/CESM system (E_CTL) realistically simulated the T1 evolution (Figures 5a–5e). The deepening of the initial trough in the first 6 h, and the development of the cutoff low, as well as its propagation are all similar to the GFS analysis (Figures 5a–5f). The trough T2 over the west coast also developed to a cutoff low 1 day later than T1 did, even though its location is slightly too far to the east and the intensity is weaker than in the GFS. The simulated precipitation associated with T1 from the WRF in the CESM/WRF system has more realistic amplitude and regional structures than the CAM (Figure 4).

[20] As a benchmark, we carried out a WRF offline simulation for the same domain with the same resolution (30 km grid spacing) driven by the GFS boundary and initial conditions (referred to as the E_ARW
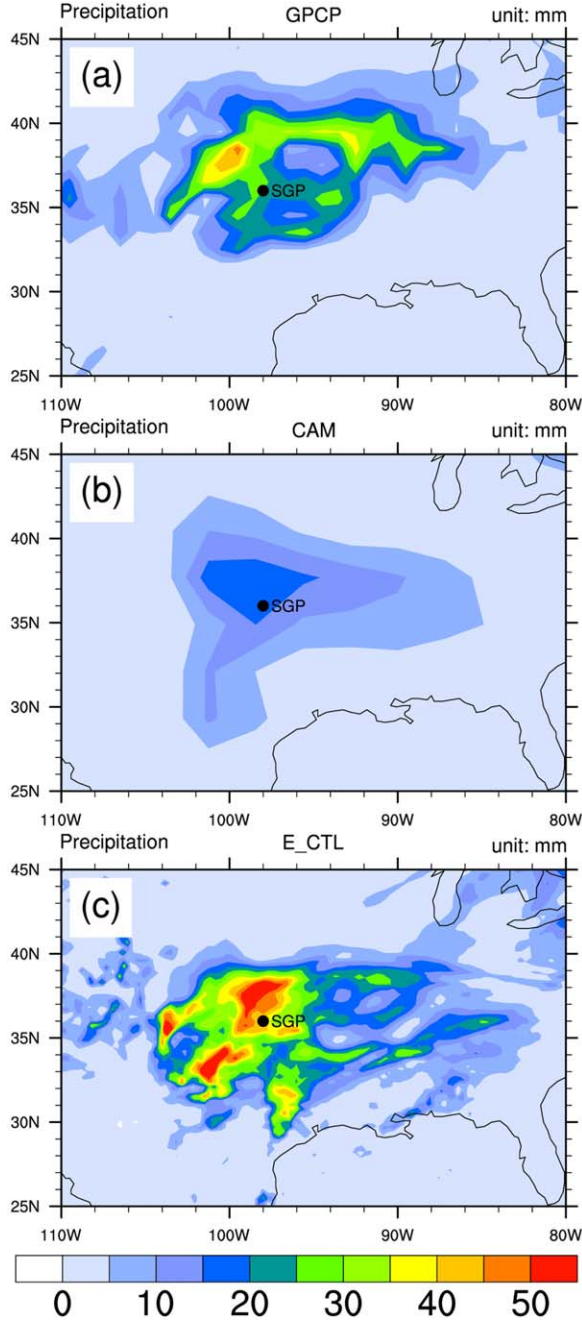
Figure 4. Total precipitation (mm) from 00 UTC 1 March to 00 UTC 4 March. (a) GPCP, (b) CAM4, and (c) E_CTL. The black dot is the center of the ARM SGP site.

simulation; Figures 5f–5j). The features from the E_ARW are very similar to those in the E_CTL. Minor difference compared to E_CTL appeared toward the end of the simulation on the upstream (west) side of the WRF domain. This is due to the impact of the upstream lateral boundary condition of CAM4.

[21] The reason why the CAM failed to simulate the cyclogenesis, even though the same coarse-resolution initial conditions were used as the WRF, can be demon-strated by using the potential vorticity diagnostics [Davis and Emanuel, 1991]. Figures 6a–6e show the evo-lution of the Ertel's potential vorticity (EPV) in CAM4 calculated from the geopotential heights in Figures 3f–3j, while Figures 6f–6j show the EPV in the WRF within the CESM. At the initial time, there is a positive vorticity maximum along the California coast. Six hours later, the shape of the EPV maximum does not change much in CAM4 and it is centered near its earlier location (40°N, 120°W), while in the WRF the EPV spatial gradient has sharpened. In the subsequent 2 days, the EPV maximum in CAM4 weakens and propa-gates eastward. In contrast, the positive maximum EPV in the WRF becomes further narrowed. Its filament forms a cyclonic hook at the south end of the EPV max-imum that corresponds to the cyclogenesis. The GFS analysis and the ARW simulations are similar to the WRF simulation and so they are not shown.

[22] The Potential Vorticity (PV) inversion technique may give some insight into the cyclonegensis. In Figure 7, we zoom in the continental United States and use 6 hourly results in the first 30 h to show the difference in the evolution of the EPV gradient between CAM4 and WRF forced by CAM4. Superimposed on the EPV are the horizontal nondivergent winds at 500 hPa derived from the EPV inversion. The balanced flow (ϕ, ψ) and the EPV, where ϕ is the geopotential height and ψ the stream function, satisfy following nonlinear equations:

$$\nabla^2\phi = \nabla \cdot f\nabla\psi + 2m^2\left[\frac{\partial^2\psi\partial^2\psi}{\partial x^2\partial y^2} - \left(\frac{\partial^2\psi}{\partial y\partial x}\right)^2\right]$$

$$\text{EPV} = \frac{g\kappa\pi}{p}\left[(f + m^2\nabla^2\psi)\frac{\partial^2\phi}{\partial\pi^2} - m^2\left(\frac{\partial^2\phi}{\partial x\partial\pi}\frac{\partial^2\psi}{\partial x\partial\pi} + \frac{\partial^2\phi}{\partial y\partial\pi}\frac{\partial^2\phi}{\partial y\partial\pi}\right)\right]$$

and the boundary condition:

$$\frac{\partial\phi}{\partial\pi} = f\frac{\partial\psi}{\partial\pi} = -\theta$$

where $\kappa = R_d/c_p$, $\pi = c_p\left(\frac{p}{p_o}\right)^\kappa$, p the pressure, m the map-scale factor, f the Coriolis parameter, θ the potential temperature, g the gravity acceleration, and x and y the coordinates. The unit is 10^{-6} m^2 s^{-1} K kg^{-1} as one potential vorticity unit (1 PVU). The equations were solved by iteration following *Davis and Emanuel* [1991]. The nondivergent wind was derived by v = k × Δψ.

[23] In CAM4, the wind merely advected the EPV eastward along with the wind. In WRF, the higher reso-lution allowed the inverted winds to simulate a conflu-ence toward the southern edge of the EPV maximum, leading to the sharpening of the EPV gradient. The westerly wind component weakened and formed an easterly wind component at 1800 UTC 1 March from the EPV maximum (Figure 7h), causing further sharp-ening of the EPV gradient and the cyclogenesis. By 0600 UTC 2 March (Figure 7i), the EPV aloft associ-ated with the cyclonic vortex began to weaken, likely because of the latent heating at midlevels. This
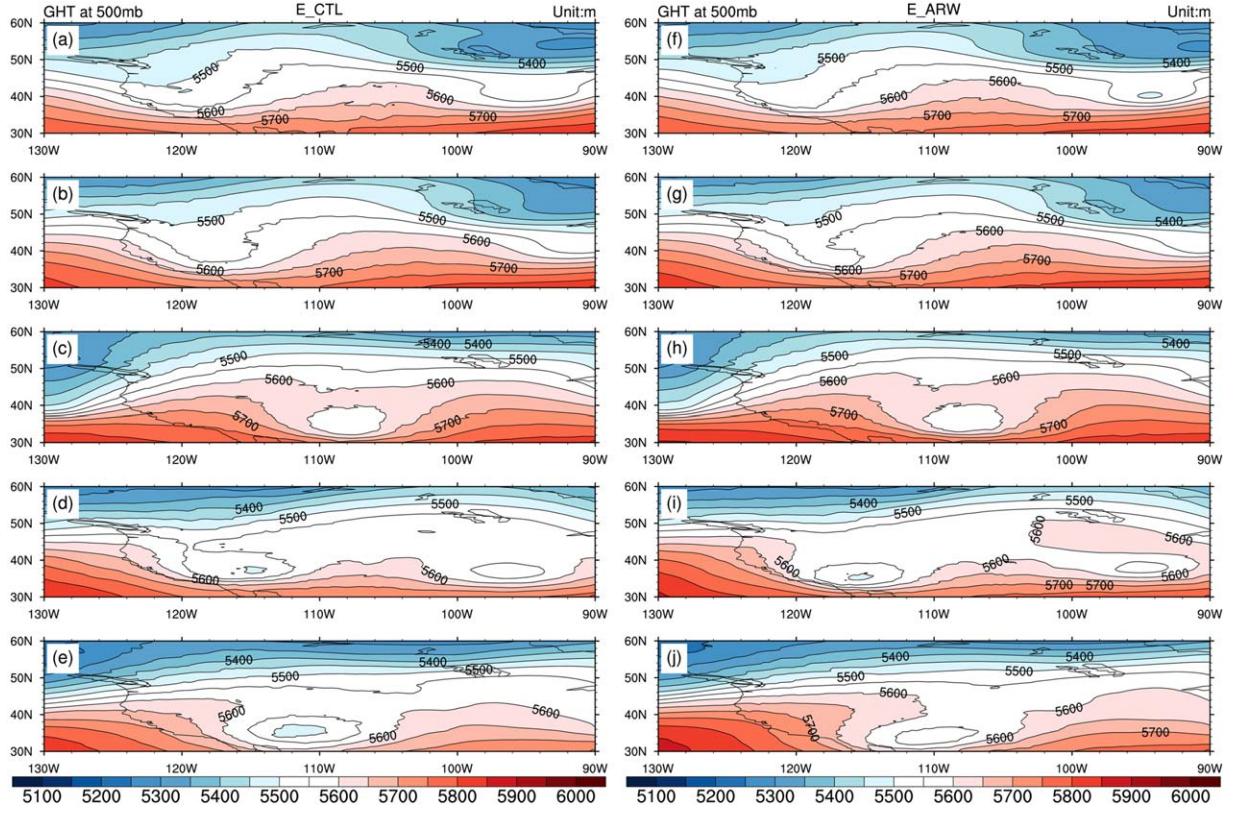
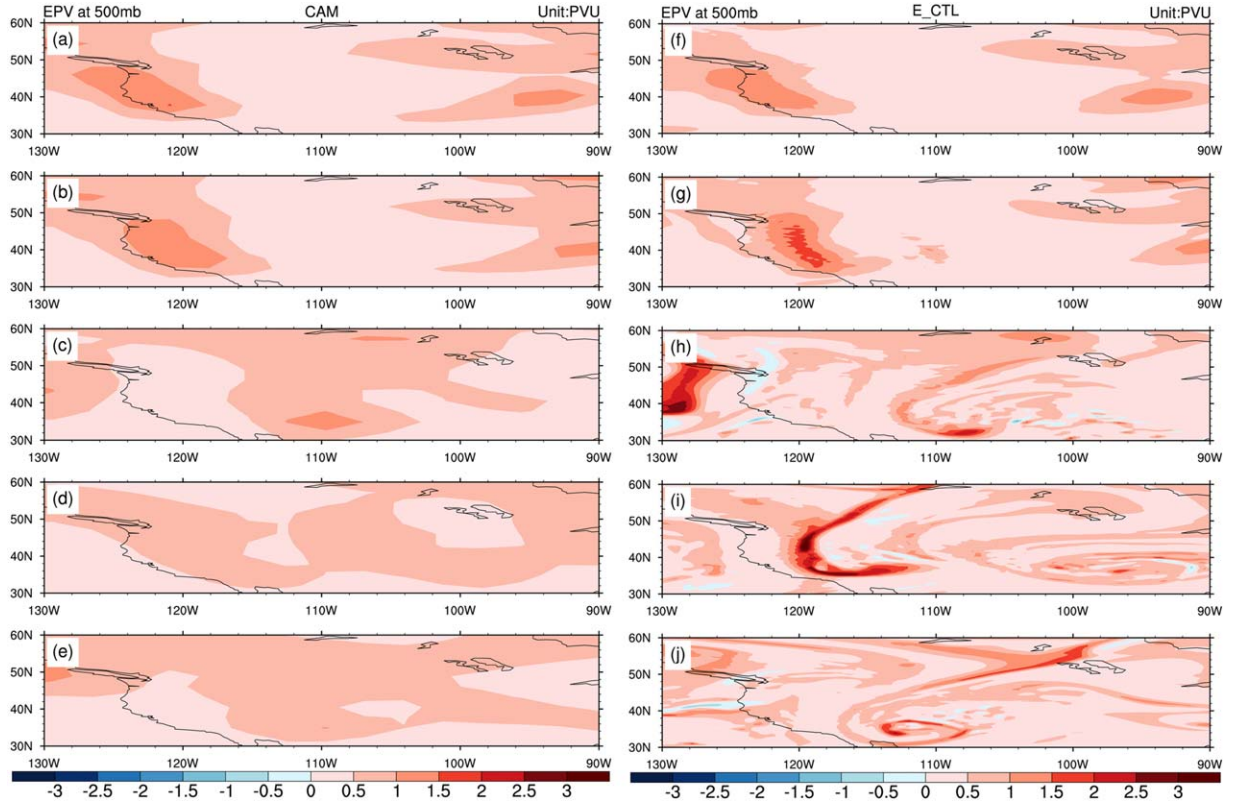**Figure 5.** Same as Figure 3 but for the (a–e) E_CTL and (f–j) E_ARW.

Figure 6. Same as Figure 3 but for EPV derived from for (a–e) the CAM4 and (f–j) the E_CTL, Unit: potential vorticity unit.
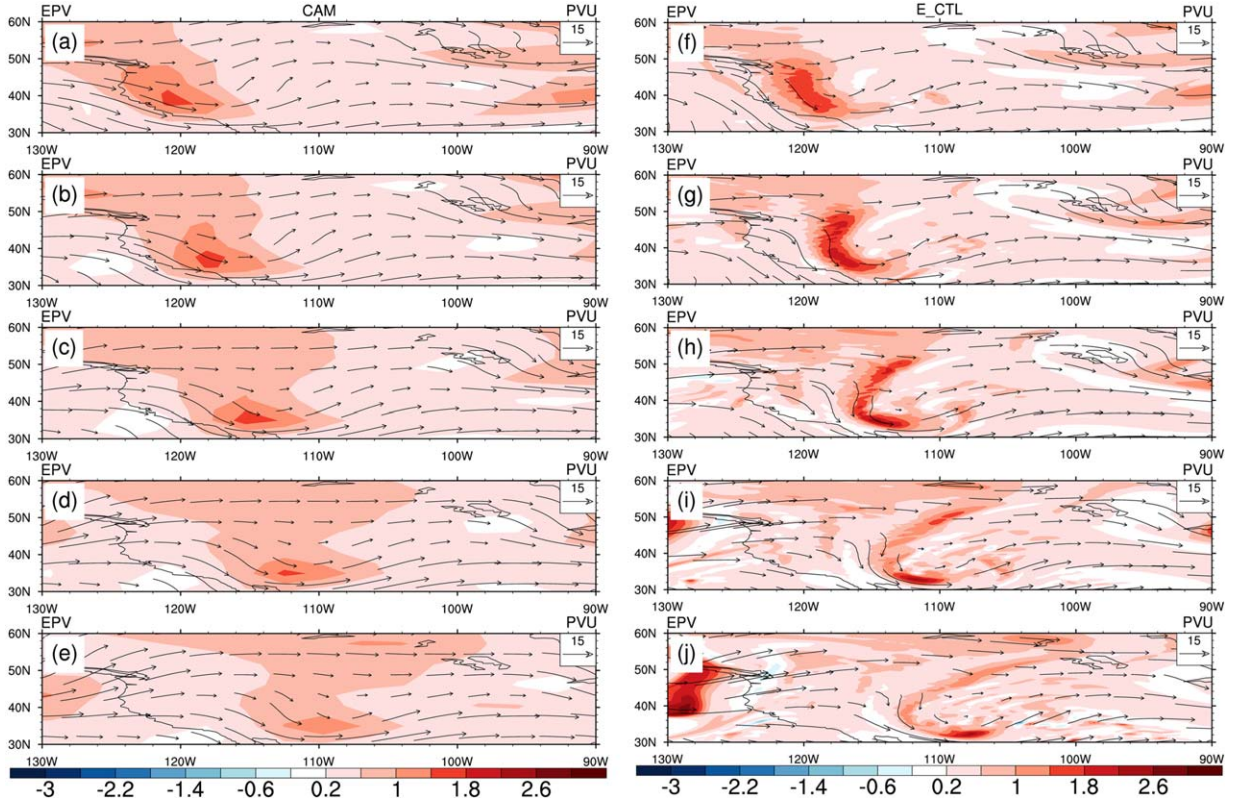
7

Figure 7. EPV with the nondivergent wind field at 500 hPa every 6 h (from the top downward) at 06 UTC, 12 UTC, 18 UTC for 1 March and 00 UTC, 06 UTC for 2 March. The EPV unit is potential vorticity unit, and the wind unit is meter per second with a reference magnitude (given in the inset) of 15 m s^{-1} for (a–e) CAM4 and (f–j) E_CTL.

development of the sharp gradient from the nonlinear flow interaction and changes from latent heat release cannot be adequately resolved in the T42 CAM.

4.2. Impact of Surface Terrain and Physical Parameterizations

[24] The above analysis suggests that model spatial resolutions played a key role in explaining the success of WRF relative to CAM4. Due to the coarse resolution, the terrain height in the CAM is lower over the Rocky Mountain than in the WRF, but is higher over the SGP and near the coast. Since the WRF surface topography is more realistic than the CAM one, we examined the terrain impact on simulations by completing an experiment ("E_Terrain") in which the WRF used the same coarse resolution terrain as CAM4. Figures 8a and 8b respectively show the terrain distributions in the two data sets. The difference of the topography on the coarse resolution grids (E_Terrain minus E_CTL) is shown in Figure 8c.

[25] Figures 9a–9e show the evolution of the 500 hPa geopotential height in the WRF with the smoother CAM topographic data. WRF can still simulate the main features of the cyclogenesis, and its features are very similar to those for E_CTL (Figures 5a–5e). Therefore, the terrain resolution does not play a major role in explaining the simulation difference between WRF and CAM4.

[26] Since CAM4 and WRF used different physical parameterizations, we conducted another experiment in which clouds, cumulus convection, and other moist physics in the WRF were turned off (E_Dry). Figures 9f–9j show the simulated evolution of the geopotential height. It is seen that the deepening of the T1 trough and the development of the cutoff low are similar in the dry model and in the full physics model (Figures 5a–5e). However, the upstream trough T2 did not develop into a cutoff low in the first 4 days, suggesting that the diabatic heating played a role there. But for T1, the dynamical process played the dominant role. This is consistent with the advection of EPV shown earlier.

4.3. Sensitivity to Resolution

[27] A series of experiments were conducted to investigate the dependence of the targeted cyclogenesis on the resolution of the nested WRF model. In one run, the WRF resolution was degraded relative to the E_CTL, while for another run the resolution was increased to see whether the simulated evolution of the two troughs in E_CTL can be further improved. Figures 10a–10e show the WRF simulation of the 500 hPa geopotential height in CESM when its resolution is degraded to 2.5° by 2.5° (E_Res1). Similar to the CAM4 simulation in Figure 3b, the WRF/CESM failed to simulate the deepening of the troughs and the cutoff
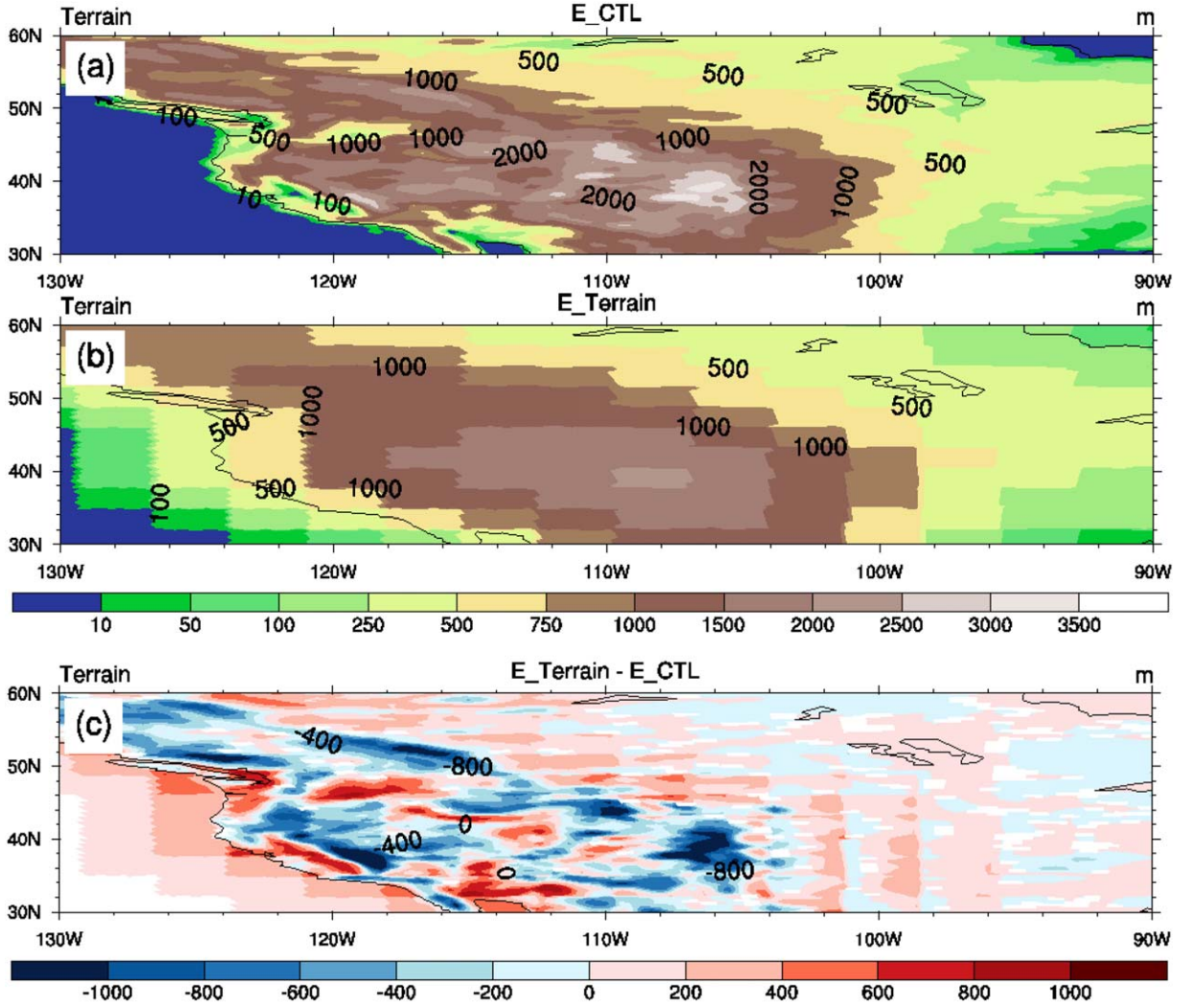
Figure 8. Surface terrain height unit (meter). (a) E_CTL, (b) E_Terrain, and (c) Difference (E_Terrain—E_CTL).

lows. This reinforces the important role of resolution in the cyclogenesis, since the WRF used different physical parameterizations from the CAM4. This is consistent with the previous studies on the sensitivity of cyclone-gensis simulation to the horizontal resolution [e.g., *Jung et al.*, 2006]. Figures 10f–10j show the WRF simulation when its spatial resolution is enhanced to 10 km (E_Res2). The time step was adjusted accordingly, and the convection scheme was not used. It is noted that this simulation is very similar to that in E_CTL (Figures 5a–5e). The higher resolution does not lead to further improvement to the intensity and propagation speed of the two cutoff lows. Other resolution sensitivity experiments (not shown) indicate that the nested model needs to have a minimum resolution of 100 km to simulate the cyclogenesis of this study in terms of a closed circulation at 500 hPa, and that higher resolution beyond the E_CTL is not necessary for the presently targeted event. This inference will clearly depend on the specific cases, applications and objectives of the nested model.

6. Summary

[28] We have described an integrated global and regional climate model in which WRF is nested within the CESM by using initial and boundary conditions with CAM, and there is data exchange between the regional WRF and the CESM using the CESM coupler. The modeling system is intended for a regional and global climate model simulation with both downscaling and upscaling capabilities.

[29] We have applied this system in one-way nesting to simulate a cyclogenesis event over the United States Southern Great Plains. The CAM4 at T42 resolution has missed the initial deepening of a midtropospheric trough and the development of a cutoff low, while the nested WRF with the same initial conditions and forced laterally by CAM4 was able to capture the main targeted features as observed. The higher resolution of the WRF allowed the sharpening of the spatial gradient of the potential vorticity, which led to the development of
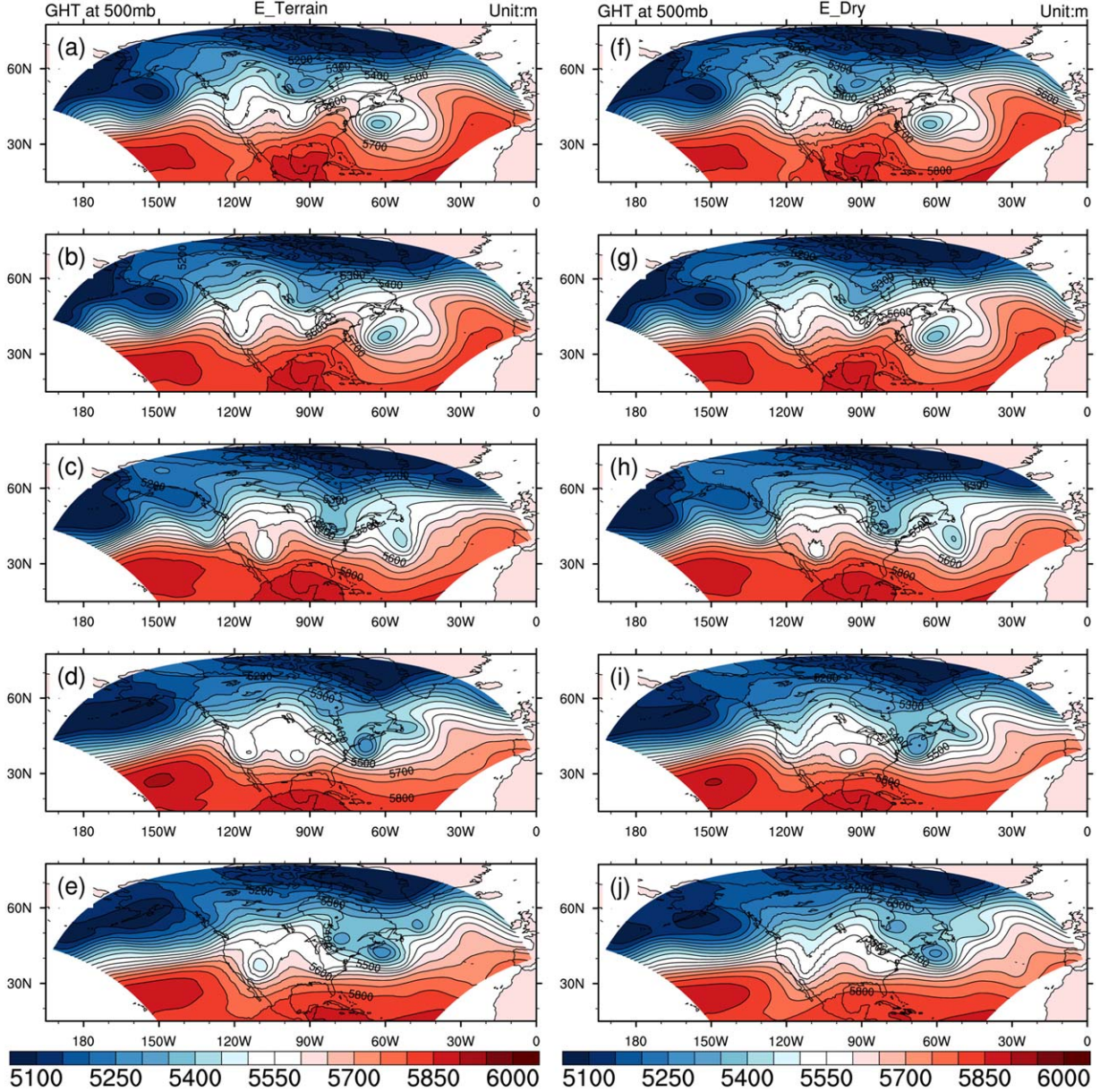
Figure 9. Same as Figure 3 but for (a–e) the E_Terrain, and (f–j) the E_Dry.

the cyclone. Sensitivity experiments are conducted with respect to the resolution of surface terrain, physical parameterization packages, and resolutions of the nested WRF. All these experiments point to the horizontal resolution as the explanation for the model's ability to simulate the cyclogenesis via the nonlinear advective interaction of the dynamics.

[30] We have not discussed the dependence of simulation results on the domain size of the nested model or of the large-scale lateral boundary, since there are many papers within the literature for these issues [e.g., *Diaconescu et al.*, 2007; *Leduce and Laprise*, 2009; *Bukovsky and Karoly*, 2011]. We expect that the optimal domain size will depend on the specific regional phenomenon that is targeted. If the domain is too small, the large-

scale lateral boundary from the global CAM4 can heavily influence the simulation, leading the system to miss the cyclogenesis. In the present case, the development of the trough associated with the targeted cyclogenesis is primarily due to the initial conditions, so the WRF E_CTL domain is sufficient. The upstream trough (T2), however, depends more on the lateral boundary. We find that when the domain size is reduced by about 40% (not shown), the upstream trough T2 within the WRF domain does not develop into a closed low with the same resolution as E_CTL because the CAM did not simulate a closed low.

[31] In this study, we have not investigated the errors in detail in the WRF itself. There is a large body of literature from WRF users and developers on this subject
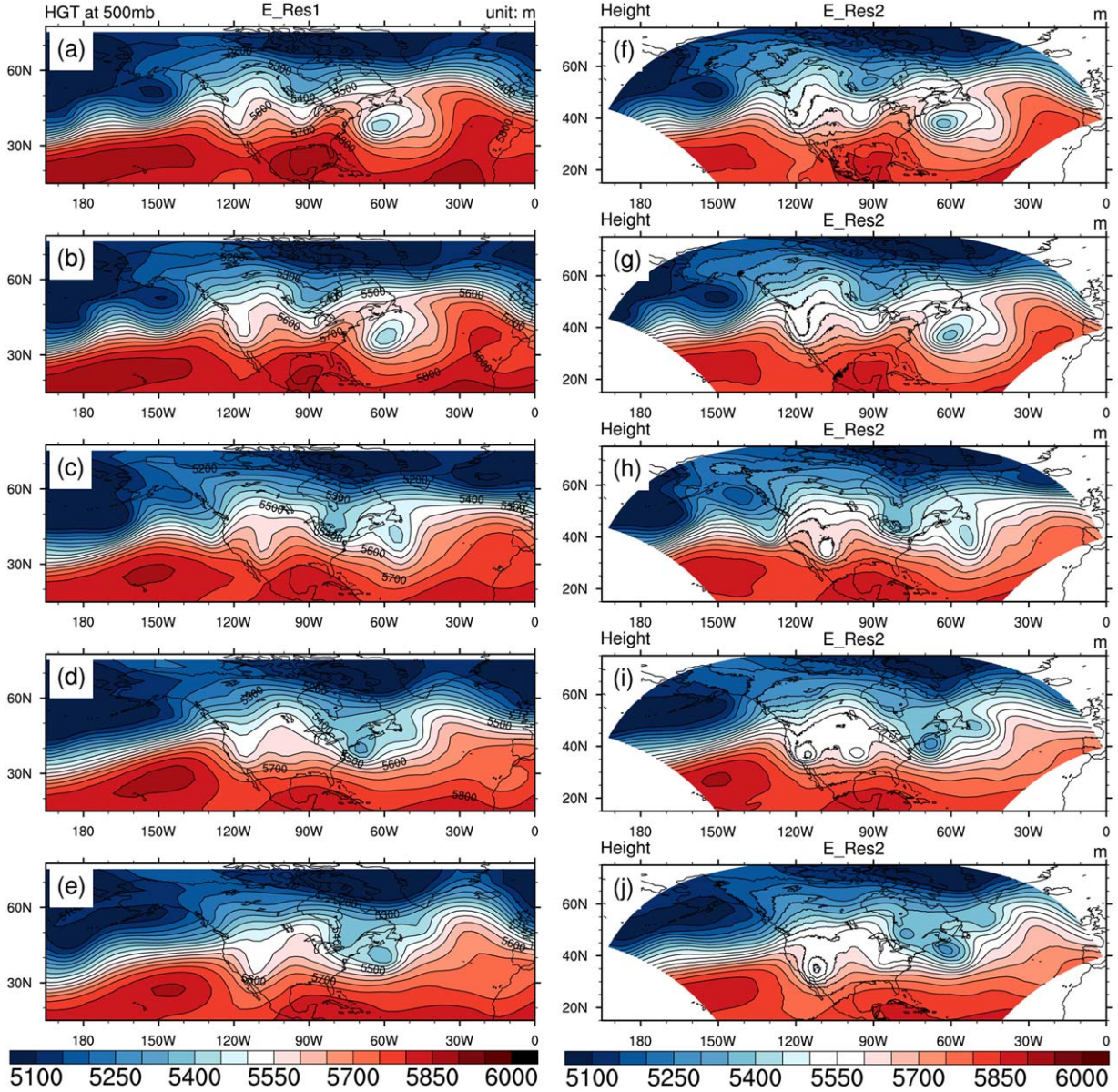
Figure 10. Same as Figure 3 but for (a–e) the E_Res1, and (f–j) the E_Res2.

[e.g., *Bukovsky and Karoly*, 2011; *Jin et al.*, 2011; *Xu and Yang*, 2012; *Liang et al.*, 2012]. It is our hope that, through the integrated WRF/CESM system, the knowledge and experience from the numerical weather prediction community can be used to aid the improvement of global climate models with regional climate simulation capabilities and skills.

[32] Obviously, as a regional climate modeling tool, we need to investigate the performance and strategy of the long-term integration of the nested model within the global model. There will be nontrivial obstacles to overcome such as the drifting of WRF from CAM [*Liang et al.*, 2012; *Xu and Yang*, 2012]. A two-way nesting may alleviate such issues and provide an alternative to improve the physical schemes of the global model by using high resolution regional information, but this will likely require years of research. We also need to carry out long-term climate simulations and apply the necessary metrics to assess it. While these are all important, case studies that target synoptic weather systems are also necessary to establish a model's credibility as a regional climate model. This paper represents one of these efforts.

References

Adler, R. F., et al. (2003), The version 2 Global Precipitation Climatology Project (GPCP) monthly precipitation analysis (1979–present), *J. Hydrometeorol.*, *4*, 1147–1167.

Anthes, R. A., Y. H. Kuo, S. Low-Nam, E. Y. Hsie, and T. M. Bettge (1989), Estimation of episodic and climatological skill and uncertainty in regional numerical models, *Q. J. R. Meteorol. Soc.*, *115*, 763–806.

Bukovsky, M. S., and D. J. Karoly (2011), A regional modeling study of climate change impacts on warm-season precipitation in the central United States, *J. Clim.*, *24*, 1985–2002.

Chen, F., and J. Dudhia (2001), Coupling an advanced land surface–hydrology model with the Penn State–NCAR MM5 modeling system, Part I: Model implementation and sensitivity, *Mon. Weather Rev.*, *129*, 569–585.

Cocke, S., and T. E. LaRow (2000), Seasonal predictions using a regional spectral model embedded within a coupled ocean–atmosphere model, *Mon. Weather Rev.*, *128*, 689–708.

Collins, W. D., et al (2004), Description of the NCAR Community Atmosphere Model (CAM3.0), *NCAR Tech. Note NCAR/TN-4641STR*, pp. 214, the National Center for Atmospheric Research, Boulder, Colo.

Craig, A. P., M. Vertenstein, and R. Jacob (2011), A new flexible coupler for earth system modeling developed for CESM and CESM1, *Int. J. High Performance Comput. Appl.*, *26*, 31–42, doi:10.1177/1094342011428141.

Davis, C., and K. A. Emanuel (1991), Potential vorticity diagnostics of cyclogenesis, *Mon. Weather Rev.*, *119*, 1929–1953.

DeWeaver, E., and C. M. Bitz (2006), Atmospheric circulation and its effect on Arctic Sea Ice in CCSM3 simulations at medium and high resolution, *J. Clim.*, *19*, 2415–2436.

Diaconescu, E. P., R. Laprise, and L. Sushama (2007), The impact of lateral boundary data errors on the simulated climate of a nested regional climate model, *Clim. Dyn.*, *28*, 333–350.

Dickinson, R. E., R. Errico, F. Giorgi, and G. Bates (1989), A regional climate model for the western United States, *Clim. Change*, *15*, 383–422.

Gent, P. R., et al. (2011), the community climate system model version 4, *J. Clim.*, *24*, 4973–4991, doi:10.1175/2011JCLI4083.1.

Giorgi, F. (1990), Simulation of regional climate using a limited area model nested in a general circulation model, *J. Clim.*, *3*, 941–963.

Giorgi, F. (1995), Perspectives for regional earth system modeling, *Global Planet. Change*, *10*, 941–963.

Grell, G. A., J. Dudhia, and D. R. Stauffer (1994), A description of the fifth-generation Penn State/NCAR Mesoscale Model (MM5), *NCAR Tech. Note NCAR/TN-398+STR*, pp. 121, the National Center for Atmospheric Research, Boulder, Colo.

He, J., G. Newby, A. Craig, J. Jackaki, and C. Zhu (2009), Developing the coupled WRF within CCSM4, paper presented at Second OFES International Workshop and ESC-IPRC Joint Workshop on Computationally-Intensive Modeling of the Climate System, Honolulu, Hawaii, 9–10 Dec, sponsored by the JAMSTEC Earth Simulator Center and the International Pacific Research Center of the University of Hawaii.

Hong, S.-Y., J. Dudhia, and S.-H. Chen (2004), A revised approach to ice microphysical processes for the bulk parameterization of clouds and precipitation, *Mon. Weather Rev.*, *132*, 103–120.

Hong, S.-Y., Y. Noh, and J. Dudhia (2006), A new vertical diffusion package with an explicit treatment of entrainment processes, *Mon. Weather Rev.*, *134*, 2318–2341.

Jin, J. M., S. Y. Wang, and R. R. Gillies (2011), An improved dynamical downscaling for the western United States, in *Climate Change: Research and Technology for Adaptation and Mitigation*, edited by J. Blanco and H. Kheradmand, pp. 23–38, InTech, Croatia.

Jung, T., S. K. Gulev, I. Rudeva and V. Soloviov (2006), Sensitivity of extratropical cyclone characteristics to horizontal resolution in the ECMWF model, *Q. J. R. Meteorol. Soc.*, *132*, 1839–1857.

Kain, J. S. (2004), The Kain–Fritsch convective parameterization: An update, *J. Appl. Meteorol.*, *43*, 170–181.

Leduce, M., and R. Laprise (2009), Regional climate model sensitivity to domain size, *Clim. Dyn.*, *32*, 833–854.

Leung, L. R., B. Kuo, and J. Tribbia (2006), Research needs and directions of regional climate modeling using WRF and CCSM, *Bull. Am. Meteorol. Soc.*, *87*, 1747–1751.

Liang, X. Z., et al. (2012). Regional climate-weather research and forecasting model (CWRF), *Bull. Am. Meteorol. Soc.*, *93*, 1363–1387.

McClean, J. L., et al. (2011), A prototype two-Decade fully-coupled fine-resolution CCSM simulation, *Ocean Modell.*, *39*, 10–30, doi:10.1016/j.ocemod.2011.02.011.

Michalakes, J., J. Dudhia, D. Gill, T. Henderson, J. Klemp, W. Skamarock, and W. Wang (2004), The Weather research and forecast model: Software architecture and performance, in *Proceeding of the Eleventh ECMWF Workshop on the Use of High Performance Computing in Meteorology, 25–29 Oct 2004*, edited by G. Mozdzynski, pp. 156–168, published by World Scientific Publishing Company, Reading, U. K.

Qian, T., A. Dai., K. E. Trenberth, and K. W. Oleson (2006), Simulation of global land surface conditions from 1948 to 2002, Part I: Forcing data and evaluations, *J. Hydrometeorol.*, *7*, 953–975.

Randall, D. A. et al. (2007), Climate models and their evaluation, in *Climate Change 2007, Working Group I: The Physical Science Basis*, pp. 589–662, Cambridge Univ. Press, Cambridge, U. K.

Reynolds, R. W., N. A. Rayner, T. M. Smith, D. C. Stokes, and W. Wang (2002), An improved in situ and satellite SST analysis for climate, *J. Clim.*, *15*, 1609–1625.

Taylor, K. E., J. S. Ronald, and G. A. Meehl (2012), An overview of CMIP5 and the experiment design, *Bull. Am. Meteorol. Soc.*, *93*, 485–498.

Taylor, M. A., and A. Fournier (2010), A compatible and conservative spectral element method on unstructured grids, *J. Comput. Phys.*, *229*, 5879–5895, doi:http://dx.doi.org/10.1016/j.bbr.2011.03.031.

U.S. National Centers for Environmental Prediction, National Weather Service, NOAA, U.S. Department of Commerce (2000), updated daily. NCEP FNL Operational Model Global Tropospheric Analyses, continuing from July 1999, Dataset ds083.2, CISL Data Support Section, Natl. Cent. for Atmos. Res., Boulder, Colo. [Available at http://dss.ucar.edu/datasets/ds083.2/.]

Wu, J. B., M. H. Zhang, and W. Y. Lin (2007), A case study of a frontal system simulated by a climate model: Clouds and radiation, *J. Geophys. Res.*, *112*, D12201, doi:10.1029/2006JD008238.

Xie, S., et al. (2005), Simulations of midlatitude frontal clouds by single-column and cloud-resolving models during the atmospheric radiation measurement March 2000 cloud intensive operational period, *J. Geophys. Res.*, *110*, D15S03, doi:10.1029/2004JD005119.

Xu, K.-M., et al. (2005), Modeling springtime shallow frontal clouds with cloud-resolving and single-column models, *J. Geophys. Res.*, *110*, D15S04, doi:10.1029/2004JD005153.

Xu, Z.-F., and Z.-L. Yang (2012), An improved dynamical downscaling method with GCM bias corrections and its validation with 30 years of climate simulations, *J. Clim.*, *25*, 6271–6286.

Corresponding author: M. Zhang, School of Marine and Atmospheric Sciences, State University of New York at Stony Brook, Stony Brook, NY 11794-5000, USA. (minghua.zhang@stonybrook.edu)